Optics EXPRESS

Development of a Doppler-broadened NICE-OHMS system for trace gas detection based on a single sideband phase modulator

JIANXIN LIU,[1,2,3] GANG ZHAO,[1,3] WEIGUANG MA,[1,3,4] AND OVE AXNER[2,5]

[1] State Key Laboratory of Quantum Optics and Quantum Optics Devices, Institute of Laser Spectroscopy, Shanxi University, Taiyuan 030006, China
[2] Department of Physics, Umeå University, SE-90187 Umeå, Sweden
[3] Collaborative Innovation Center of Extreme Optics, Shanxi University, Taiyuan 030006, China
[4] mwg@sxu.edu.cn
[5] ove.axner@umu.se

Abstract: To expand the applicability of noise-immune cavity-enhanced optical heterodyne molecular spectrometer (NICE-OHMS), a universal system incorporating a fiber-coupled single-sideband modulator (f-SSM) for control of the laser frequency has been developed. A homemade PID servo mainly composed of two integrators has been designed, resulting in a locking bandwidth of 170 kHz and a continuous tuning range of 2.2 GHz. The system exhibits a noise-equivalent Doppler-broadened absorption limit of 8.0×10^{-14} cm^{-1} for an integration time of 64 s. Since the f-SSM is the sole external frequency actuator, this opens up for NICE-OHMS based on a multitude of laser systems.

1. Introduction

Benefiting from its superior characteristics, including high sensitivity and resolution, good selectivity, fast response and non-invasive measurement, laser absorption spectroscopy (LAS) has been applied to various fields, e.g. air pollution monitoring [1], industrial process control [2], medical diagnostics [3], isotope measurement [4], national defense security [5], and Mars methane detection [6]. There are also increasing interests in its use for fundamental research fields, e.g. for spectra parameter measurements [7], as optical frequency standard [8], and for ultra-cold atomic and molecular spectroscopy [9]. Up to now, the minimum detectable laser intensity attenuation rate ($\Delta I/I$, where I is the laser intensity) due to absorption, also referred to as the minimum detectable absorption (MDA), range, for different LAS techniques, from 10^{-3} to 10^{-13}.

The simplest and most basic LAS technique is slow-scanned direct absorption spectroscopy (DAS), which has a MDA of 10^{-3}. One way to improve on this is to utilize a fast scanning scheme [10] or a modulation/demodulation [11] technique since such can encode the absorption information into audio/radio frequency range where the amount of technical noise is low. This reduces the $1/f$ noise and can provide an MDA in the 10^{-5}–10^{-6} range.

Another way to improve on LAS techniques is to increase the interaction length between the laser light and the target molecules by using a multipass cell [12] or a Fabry-Pérot (F-P) cavity [13]. This can increase the sensitivity by several orders of magnitude.

Noise-immune cavity enhanced optical heterodyne molecular spectrometry (NICE-OHMS), based on a combination of cavity enhanced absorption spectroscopy (CEAS) and frequency modulation spectroscopy (FMS), is the most sensitive LAS technique. In this technique, which uses the Pound-Drever-Hall (PDH) and the DeVoe-Brewer (DVB) techniques, all components of a frequency-modulated laser are simultaneously made resonant with longitudinal modes of a high

#437893 https://doi.org/10.1364/OE.437893
Journal © 2021 Received 15 Jul 2021; accepted 14 Nov 2021; published 7 Dec 2021

Optics EXPRESS

finesse F-P cavity. Benefiting from this, NICE-OHMS is immune to frequency-to-amplitude noise.

In its early days, based on a fixed-frequency ND:YAG laser, NICE-OHMS was utilized by Ye, Ma and Hall as a frequency reference by addressing a sub-Doppler (sD) feature in a C_2HD transition at 1064 nm [14]. In that realization, it demonstrated an astonishing noise equivalent absorption limit (NEAL) of 10^{-14} cm^{-1} over 1 s integration time. During the subsequent years, for increased applicability and for a variety of applications (e.g. as optical frequency standard, for molecular or ionic spectroscopy, for spectral parameter measurements, and for trace gas detection), NICE-OHMS was realized in a multitude of wavelength ranges (primarily in the NIR and MIR wavelength ranges) around different kinds of tunable lasers, e.g. external cavity diode lasers [15], Ti:sapphire lasers [16], DFB lasers [7,17], fiber lasers [18] and whispering gallery mode lasers [19], quantum cascade lasers [20] and optical parametric oscillators [21]. In 2018, Zhao et al. pushed the detection sensitivity of Doppler broadened (Db) NICE-OHMS realized around a F-P cavity with a finesse of 55000 by using balance detection technique to the shot noise level [22].

Despite that the NICE-OHMS technique is claimed to be noise-immune, the immunity is adversely broken if any wavelength-dependent losses are present, either from absorption of the intracavity gas or from the optical system. This implies that it is still of importance to lock the frequencies of the laser components to those of the cavity mode as tightly as possible. This requires, for the PDH locking, both a high gain at low frequencies and a large locking bandwidth. To achieve this, usually more than one frequency actuator is utilized, of which at least one is a part of the laser system. For example, in fiber laser based NICE-OHMS systems, which have demonstrated the most sensitive detection of trace gases, due to the low-pass response of the piezoelectric transducer (PZT) of the laser, an external acoustic optical modulator (AOM) is used to ensure a locking bandwidth larger than 100 kHz. This implies that the performance of the system partly is given by the properties of the laser system (e.g. its slow tunability) and partly by the AOM.

In 2019, to simplify the locking system, Zhou et al. replaced the two frequency actuators by a single fiber single-sideband electro-optic-modulator (f-SSM) [23]. An f-SSM is composed of two Mach-Zehnder (MZ) interferometers, each driven by a radio frequency (RF) source. By properly relating the phase difference of two RF signals to each other such a system can produce a single sideband. The frequency of the output from such a device can then be shifted by controlling the driving RF frequency. Since the MZ interferometers can be modulated at high MHz frequencies with the range of dozens of GHz, an f-SSM can be detuned at significantly higher frequencies than AOMs. Implementing an f-SSM into a NICE-OHMS system vouches for a more robust and versatile NICE-OHMS system (better locking and larger scanning range). The universality of the f-SSM based NICE-OHMS have been tested by various types of lasers.

However, in the initial work, which utilized a relative low finesse cavity (finesse: 2300), because of an insufficient gain of the PID at lower frequency, the tunability of the laser frequency was limited whereby only sD signals could be addressed (in that case, in that work, used as an absolute optical frequency for atmospheric Lidar). However, the sD signal is highly sensitive to a multitude of parameters, including laser intensity, light polarization, gas pressure and a gas exchange rate, which introduce difficulties to quantify the targeted gas. Since the degree of saturation is inversely proportional to the square of molecular dipole moment, high laser power is indispensable to stimulate saturation absorption, especially for the molecule with weak dipole moment like CO_2. What's more, the refined broadening, such as power broadening and transit time broadening, get noticeable or even dominant under Doppler-free scheme thus adversely affecting the absorption profile and, additionally, complicating the modelling of the signal. In conclusion, sD detection is not preferred over Db detection when trace gas detection is performed.

Optics EXPRESS

In this work, a universal NICE-OHMS setup for Db detection with a high finesse cavity has been constructed around a commercial f-SSM. A PID servo for the PDH locking with considerable gain at low frequency and a wide locking bandwidth has been designed. Its performance for Db NICE-OHMS detection is scrutinized by addressing trace concentrations of acetylene. Finally, the sensitivity of the spectrometer is evaluated by use of an Allan-Werle analysis.

2. Experimental setup

The experimental setup for f-SSM based Db NICE-OHMS, shown in Fig. 1, is similar to that in a previous work [23], with the exception for a few minor alterations. In short, the light, output from an erbium-doped fiber laser (EDFL, Adjustik E15 PztS PM, NKT Photonics), emitting light at around 1531 nm and addressing an acetylene transition at 6531.78 cm^{-1} with a line strength of 4.0×10^{-21} $cm^{-1}/(mol\cdot cm^{-2})$, was sequentially passed through an f-SSM (MU-SSB-N-15-PM-FCAPC, Beijing Keyang Photonics) driven by a voltage controlled oscillator (VCO, 108648-HMC586LC4B, Analog Devices), an erbium-doped fiber amplifier (EDFA) to amplify and stabilize the laser power, and a fiber-coupled electro optic modulator (f-EOM) with proton exchanged waveguide (to suppress the residual amplitude modulation [24]) before it is sent into free space by a fiber collimator. Two modulation frequencies at 20 MHz and 381 MHz were imposed on the laser light by the f-EOM for PDH and frequency modulation spectroscopy (FMS) with modulation indices of 0.1 and 1, respectively. Before impinging onto the cavity, the laser passed through a mode-matching lens (ML), a half wave plate (λ/2), a polarization beam splitter (PBS), and a quarter-wave plate (λ/4). The cavity, composed of two high reflection mirrors, has a finesse of 55 000. The distance between the two mirrors is 39.4 cm, providing a free space range (FSR) of 381 MHz.

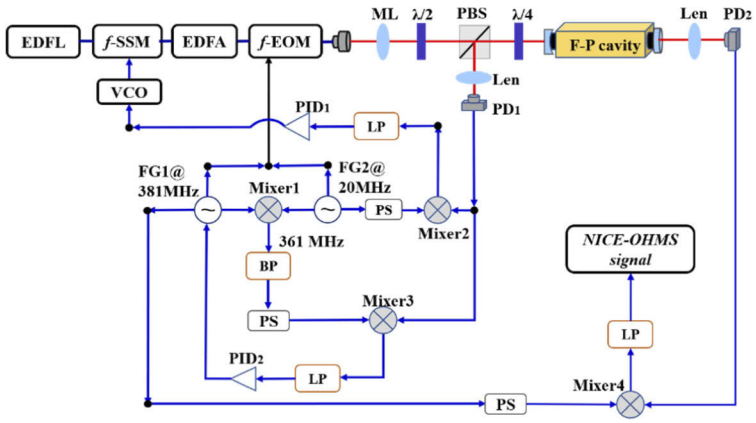

Fig. 1. Schematic illustration of the f-SSM based NICE-OHMS system. It comprises the following items: EDFL, Er-doped fiber laser; f-SSM, fiber coupled single sideband modulator; EDFA, Er-doped fiber amplifier; VCO, voltage control oscillation; f-EOM, fiber coupled electro-optic modulator; ML, mode matching lens; Len, focusing lens; λ/2, half-wave plate; PBS, polarization beam splitter; λ/4, quarter-wave plate; $PD_{1,2}$, photodetector; PS, phase shifter; LP, low pass filter; BP, bandwidth filter; and $FG_{1,2}$, frequency generator.

The reflection of the cavity was deflected by the PBS to a photodetector (PD_1), whose signal is demodulated at 20 and 361 MHz to generate error signals for the PDH and the DVB locking processes, respectively, where the latter is used to lock the modulation frequency of the FMS to the cavity FSR so that all components of the FMS are simultaneously resonant with their corresponding cavity longitudinal modes. In this setup, the VCO, which, with a modulation bandwidth of 800 kHz, drives the f-SSM, is the only unit that controls the laser frequency for

Optics EXPRESS

both laser wavelength scan and frequency locking. The NICE-OHMS signal finally, is obtained by demodulating the cavity transmitted signal from PD_2 at the modulation frequency of the FMS.

3. Locking procedure

3.1. Transfer function of the VCO controlled f-SSM

The transfer function of the combination of the VCO and the f-SSM was measured by using the comb-like cavity transmission modes as a frequency ruler. Bode plots of the transfer function are shown in Fig. 2, where the panels (a) and (b) display the normalized gain and phase shift of transfer function as functions of the driving frequency, respectively. The red curves show the corresponding theoretical fittings of a third-order low pass filter. As can be seen from the figure, the amplitude response is constant and the phase shift remains restricted for frequencies up to 100 kHz. The bandwidth is around 800 kHz, which is larger than the bandwidth of the AOM in the conventional fiber laser based NICE-OHMS [25]. This implies that the system is expected to have better locking performance than the conventional fiber laser based NICE-OHMS.

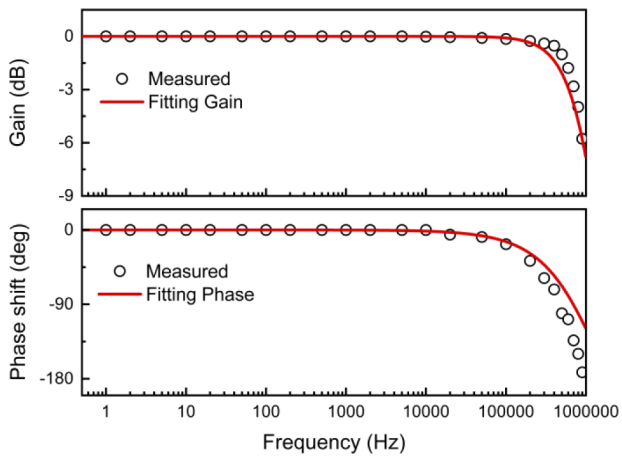

Fig. 2. Panel (a): The amplitude and, panel (b), the phase shift of the f-SSM. The black open markers represent the measured entities, while the red solid curves display the expected response of a third-order low pass filter.

3.2. Design of PID servo

With the knowledge of the response of each unit in the feedback loop (as shown in Fig. 3), a PID servo to lock the laser to the high finesse FP cavity was designed. The transfer function of the cavity, which is plotted as the red solid curves in Fig. 3 [the gain and phase shift in the panels (a) and (b), respectively], was modeled as a low pass filter with a 3 dB frequency equal to a cavity mode width of 3.45 kHz. The f-SSM response is shown by the blue curves. The curves in magenta show the transfer function of the PID servo, which consists of two active integrators at the corner frequencies of 48 Hz and 36 kHz, respectively, to ensure substantial gain at low frequency region and two phase leads. Another combination of electronic passive low-pass filter and phase lead, which is used to avoid oscillations of the loop and significantly improves the locking performance, has corner frequencies of 10 Hz and 1 kHz, respectively. The responses of the open loop without and with the integrators on, which comprises the responses of the cavity, the f-SSM model, and the PID circuit, are shown by the black solid curve and black dash dot curve in Fig. 3, respectively. They possess a substantial gain in the low frequency domain (larger than 200 dB at 1 Hz with integrators on) and result in a servo bandwidth of 170 kHz. Moreover,

Optics EXPRESS

at unit gain, it has a sufficient phase margin that is equal to 40 degrees, which guarantees a stable and robust laser-to-cavity locking.

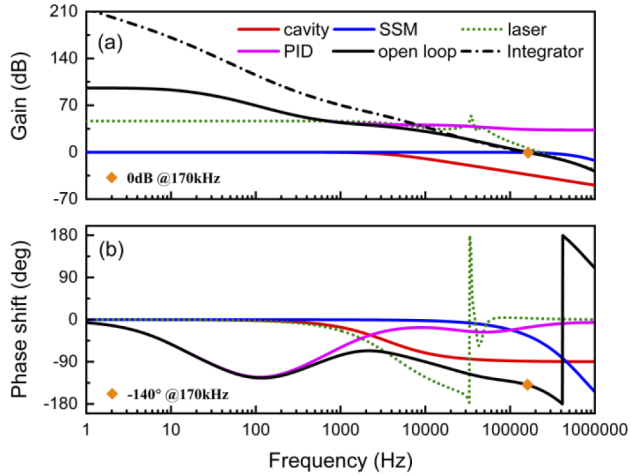

Fig. 3. Bode plot with gain and phase development of the controller for the PDH locking scheme used. The magenta curves show the PID comprising two active integrators to provide high gain at low frequencies. The black solid curves show the open loop of the feedback system, including the response of the cavity (red line), the f-SSM model (blue line) and the PID. By this, a PID servo loop with gain larger than 200 dB at 1 Hz and with 40 degrees phase margin at 170 kHz (the 0 dB point) were realized.

As a comparison, the doted green curves in Fig. 3 represent the transfer function of the fiber laser PZT. Owing to its low pass filter behavior and resonances at 35 kHz and 46 kHz, respectively, the bandwidth of the feedback servo used with the laser PZT is often limited to below 1 kHz.

3.3. Evaluation of the locking

To assess the locking performance, the frequency deviations between the laser and the cavity mode and between the cavity FSR and the modulation frequency, were deduced from the error signals of

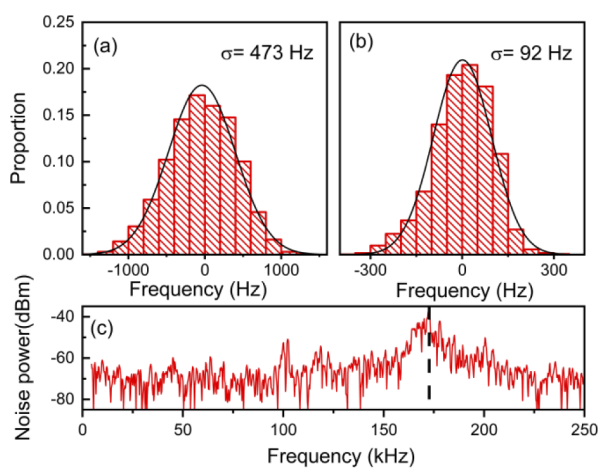

Fig. 4. Frequency distributions of the error signals of the (a) PDH and (b) DVB locking. The black solid curves represent Gaussian fits. The σ represent the FWHM of the fits. Panel (c) displays the frequency noise spectra of the PDH locking.

Optics EXPRESS

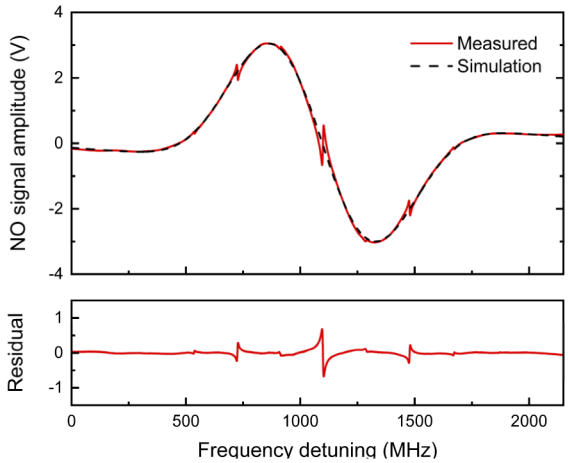

Fig. 5. Panel (a): The red solid and the black dashed curves, the measured and a fitted theoretical Db NICE-OHMS signals; Panel (b): the residual of the fit.

the PDH and DVB circuits, respectively. The frequency calibrations of the error signals originate from the odd-symmetry error signals when scanning the laser or the modulation frequency, respectively, whose peak-to-peak voltage amplitude corresponds to a frequency deviation equal to the FWHM of cavity mode (6.9 kHz in our case). The frequency distributions of the PDH and DVB error signals during locking are drawn as histogram in the Figs. 4(a) and (b), respectively. The solid curves are the fits of a Gaussian distribution function. The retrieved standard frequency deviations, i.e. the σ, were found to be 473 and 92 Hz respectively. The frequency spectrum of the PDH error signal when both locking processes are activated are drawn in Fig. 4(c). The bump at 170 kHz (marked by a black dashed line) indicates the bandwidth of PID servo loop.

4. Db NICE-OHMS signal and detection sensitivity

4.1. Db NICE-OHMS

Due to the high gain of the PID servo at low frequencies and the wide tuning range of the f-SSM, a frequency scan range of 2.2 GHz, over which a high-contrast Db NICE-OHMS signal was retrieved, could be obtained. To assess the performance of the system, the cavity was filled with 10 ppm C_2H_2 at 100 mTorr. With an incident laser power to the cavity of 2.4 mW, the intracavity power built up to more than 10 W, which provided optical saturation of the transition addressed. The red curve in Fig. 5 displays the transmitted Db NICE-OHMS signal at dispersion phase (averaged 5 times), while the black dashed curve depicts a fit of the expected Db NICE-OHMS signal based on a Voigt line shape function with pressure broadening coefficients taken from the HITRAN database [26]. The fitting residual is shown in the lower panel. Except for the sub-Doppler features, which were not considered in the fitting model, the fitting indicates a good agreement between theory and measurement. This signal was used to calibrate the response of the system.

4.2. Detection sensitivity

The detection sensitivities of two different experimental schemes [f-SSM-equipped and a combination of PZT and AOM controlled (denoted “traditional”) Db NICE-OHMS] were evaluated by the use of Allan-Werle plots. To assess the ultimate detection sensitivities of the systems, the NICE-OHMS signal was measured with the two detection schemes without gas for

Optics EXPRESS

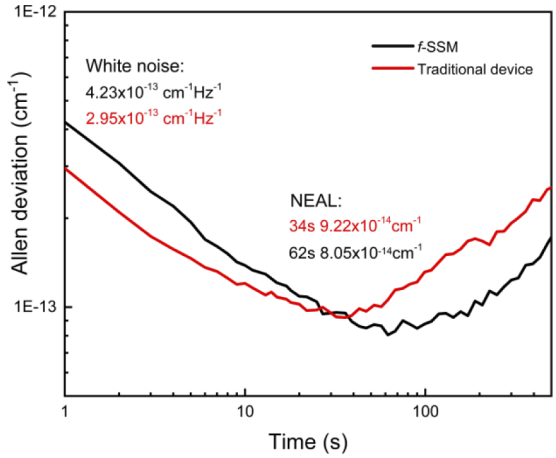

Fig. 6. Allen-Werle plot of the empty-cavity response of traditional and f-SSM-equipped Db NICE-OHMS, respectively.

more than 5 hours. The red and the black curves in Fig. 6 show the corresponding Allan-Werle plots for the traditional and the f-SSM-based NICE-OHMS setup.

Although the responses for the two realizations are clearly dissimilar, their differences are not substantial: The white noise response, dominating the curve for integration times up to around 30 s, is slightly poorer for the f-SSM equipped system than for the traditional setup (4.2 and 3.0 $\times 10^{-13}$ cm^{-1} Hz^{-1}, respectively). The cause for this is attributed to the fact that the f-SSM, which comprises a multitude of fiber components, introduce a higher level of phase noise in the NICE-OHMS dispersion signal than what a single AOM does. The long-term response, which takes place for integration times above 40 s, is better for the f-SSM system than for the traditional setup. This is attributed to the fact that there are fewer frequency actuators in the f-SSM setup.

The traditional setup provides an optimum NEAL of 9.2×10^{-14} cm^{-1} for an integration time of 34 s. For the case with the f-SSM based setup, the NEAL was found to be 8.0×10^{-14} cm^{-1} at 64 s. For a sample pressure of 70 Torr, this corresponds to a minimum detectable C_2H_2 concentration of 290 ppq (parts-per-quadrillion, 1:10^{-15}). This indicates that the f-SSM, which replaces the traditional frequency actuators with considerable tunability in NICE-OHMS, does not significantly deteriorate the analytical performance of the NICE-OHMS system.

5. Conclusion

A NICE-OHMS spectrometer for Db trace gas detection has been developed around a f-SSM, which acts as a sole actuator of the frequency of the laser light. To ensure a robust locking, a homemade PID servo loop with a bandwidth of 170 kHz was designed. With sufficient gain at low frequency of the PID servo, a robust locking of the laser light to the cavity modes a high finesse (~55 000) FP cavity could be obtained.

Two different NICE-OHMS realizations were compared; one with an f-SSM as the sole frequency actuator, and one in which the frequency control was made through the PZT in the laser (for slow frequencies) and an AOM (for higher). It was found that the two systems have similar behavior.

The locking performances of the f-SSM-based system were analyzed by the frequency distribution of the in-loop noise, resulting in standard deviations of 473 and 92 Hz for PDH and DVB locking processes, respectively. The f-SSM could also provide a laser frequency scanning range of 2.2 GHz, which is sufficient to obtain a full Db NICE-OHMS signal. The detection

Optics EXPRESS

sensitivity of the spectrometer, analyzed by an Allen-Werle plot, showed a minimum NEAL of 8.0×10^{-14} cm^{-1} for an integration time of 64 s.

Since the f-SSM is a single widely scannable external frequency actuator, this work thus demonstrates that the NICE-OHMS technique can be used with a large variety of laser sources, not only the narrow-linewidth fiber-lasers used in this realization, but also other types, including fix frequency lasers, for high sensitive Db-detection.

Funding. National Natural Science Foundation of China (61875107, 61905134, 61905136); Vetenskapsrådet (621-2015-04374); Opening Foundation of Key Laboratory of Laser & Infrared System (Shandong University).

Acknowledgments. Jianxin thanks China Scholarship Council (CSC) for support.

Disclosures. The authors declare no conflicts of interest.

Data availability. Data underlying the results presented in this paper are not publicly available at this time but maybe obtained from the authors upon reasonable request.

References

1. J. L. Jimenez, G. J. McRae, D. D. Nelson, M. S. Zahniser, and C. E. Kolb, "Remote sensing of NO and NO_2 emissions from heavy-duty diesel trucks using tunable diode lasers," Environ. Sci. Technol. **34**(12), 2380–2387 (2000).
2. G. B. Rieker, J. B. Jeffries, R. K. Hanson, T. Mathur, M. R. Gruber, and C. D. Carter, "Diode laser-based detection of combustor instabilities with application to a scramjet engine," Proc. Combust. Inst. **32**(1), 831–838 (2009).
3. M. Azhar, J. Mandon, A. H. Neerincx, Z. Liu, J. Mink, P. J. F. M. Merkus, S. M. Cristescu, and F. J. M. Harren, "A widely tunable, near-infrared laser-based trace gas sensor for hydrogen cyanide (HCN) detection in exhaled breath," Appl. Phys. B **123**(11), 268 (2017).
4. A. J. Fleisher, D. A. Long, Q. Liu, L. Gameson, and J. T. Hodges, "Optical Measurement of Radiocarbon below Unity Fraction Modern by Linear Absorption Spectroscopy," J. Phys. Chem. Lett. **8**(18), 4550–4556 (2017).
5. D. C. Meier, K. D. Benkstein, W. S. Hurst, and P. M. Chu, "Fourier Transform Infrared Absorption Spectroscopy for Quantitative Analysis of Gas Mixtures at Low Temperatures for Homeland Security Applications," J. Test. Eval. **45**(3), 20150382 (2017).
6. M. L. Silva, "*Spectroscopic investigations of the $\widetilde{X}$ and $\tilde{A}$ state dynamics of 13C2H2*," (Massachusetts Institute of Technology, Cambridge, 2002).
7. A. Foltynowicz, J. Wang, P. Ehlers, and O. Axner, "Distributed-feedback-laser-based NICE-OHMS in the pressure-broadened regime," Opt. Express **18**(18), 18580–18591 (2010).
8. J. Wang, Y. R. Sun, L. G. Tao, A. W. Liu, and S. M. Hu, "Communication: Molecular near-infrared transitions determined with sub-kHz accuracy," J Chem Phys **147**(9), 091103 (2017).
9. S. Mauger, J. Millen, and M. P. A. Jones, "Spectroscopy of strontium Rydberg states using electromagnetically induced transparency," J. Phys. B-At. Mol. Opt **40**(22), F319–F325 (2007).
10. K. O. Douglass, S. E. Maxwell, G.-W. Truong, R. D. van Zee, J. R. Whetstone, J. T. Hodges, D. A. Long, and D. F. Plusquellic, "Rapid scan absorption spectroscopy using a waveform-driven electro-optic phase modulator in the 1.6-1.65 um region," J. Opt. Soc. Am. B **30**(10), 2696–2703 (2013).
11. D. S. Bomse, A. C. Stanton, and J. A. Silver, "Frequency-modulation and wavelength modulation spectroscopies-comparison of experimental methods using a lead-salt diode-laser," Appl. Opt. **31**(6), 718–731 (1992).
12. C. Robert, "Simple, stable, and compact multiple-reflection optical cell for very long optical paths," Appl. Opt **46**(22), 5408–5418 (2007).
13. G. Gagliardi and H. P. Loock, "Cavity-Enhanced Spectroscopy and Sensing," (2014).
14. J. Ye, L. S. Ma, and J. L. Hall, "Sub-Doppler optical frequency reference at 1.064 um by means of ultrasensitive cavity-enhanced frequency modulation spectroscopy of a C_2HD overtone transition," Opt. Lett. **21**(13), 1000–1002 (1996).
15. C. Ishibashi and H. Sasada, "Highly sensitive cavity-enhanced sub-Doppler spectroscopy of a molecular overtone band with a 1.66 µm tunable diode laser," Jpn. J. Appl. Phys. **38**, 920–922 (1999).
16. J. Bood, A. McIlroy, and D. L. Osborn, "Measurement of the sixth overtone band of nitric oxide, and its dipole moment function, using cavity-enhanced frequency modulation spectroscopy," J. Chem. Phys **124**(8), 084311 (2006).
17. E. A. Curtis, G. P. Barwood, G. Huang, C. S. Edwards, B. Gieseking, and P. J. Brewer, "Ultra-high-finesse NICE-OHMS spectroscopy at 1532 nm for calibrated online ammonia detection," J. Opt. Soc. Am. B **34**(5), 950–958 (2017).
18. F. M. Schmidt, A. Foltynowicz, W. Ma, and O. Axner, "Fiber-laser-based noise-immune cavity-enhanced optical heterodyne molecular spectrometry for Doppler-broadened detection of C_2H_2 in the parts per trillion range," J. Opt. Soc. Am. B **24**(6), 1392–1405 (2007).
19. G. Zhao, T. Hausmaninger, W. Ma, and O. Axner, "Whispering-gallery-mode laser-based noise-immune cavity-enhanced optical heterodyne molecular spectrometry," Opt. Lett. **42**(16), 3109–3112 (2017).
20. M. S. Taubman, T. L. Myers, B. D. Cannon, and R. M. Williams, "Stabilization, injection and control of quantum cascade lasers, and their application to chemical sensing in the infrared," Spectrochimi. Acta. Part. A **60**(14), 3457–3468 (2004).

Optics EXPRESS

21. T. Hausmaninger, I. Silander, and O. Axner, "Narrowing of the linewidth of an optical parametric oscillator by an acousto-optic modulator for the realization of mid-IR noise-immune cavity-enhanced optical heterodyne molecular spectrometry down to 10−10 cm-1 Hz-1/2," Opt. Express **23**(26), 33641–33655 (2015).
22. G. Zhao, T. Hausmaninger, W. Ma, and O. Axner, "Shot-noise-limited Doppler-broadened noise-immune cavity-enhanced optical heterodyne molecular spectrometry," Opt. Lett. **43**(4), 715–718 (2018).
23. Y. Zhou, J. Liu, S. Guo, G. Zhao, W. Ma, Z. Cao, L. Dong, L. Zhang, W. Yin, Y. Wu, L. Xiao, A. Ove, and S. Jia, "Laser frequency stabilization based on an universal sub-Doppler NICE-OHMS instrumentation for the potential application in atmospheric Lidar," Atmos. Meas. Tech. **12**(3), 1807–1814 (2019).
24. I. Silander, P. Ehlers, J. Wang, and O. Axner, "Frequency modulation background signals from fiber-based electro optic modulators are caused by crosstalk," J. Opt. Soc. Am. B **29**(5), 916–923 (2012).
25. P. Ehlers, I. Silander, J. Wang, and O. Axner, "Fiber-laser-based noise-immune cavity-enhanced optical heterodyne molecular spectrometry instrumentation for Doppler-broadened detection in the 10(12 cm-1 Hz-1/2 region," J. Opt. Soc. Am. B **29**(6), 1305–1315 (2012).
26. I. E. Gordon, L. S. Rothman, C. Hill, R. V. Kochanov, Y. Tan, P. F. Bernath, M. Birk, V. Boudon, A. Campargue, K. V. Chance, B. J. Drouin, J. M. Flaud, R. R. Gamache, J. T. Hodges, D. Jacquemart, V. I. Perevalov, A. Perrin, K. P. Shine, M. A. H. Smith, J. Tennyson, G. C. Toon, H. Tran, V. G. Tyuterev, A. Barbe, A. G. Császár, V. M. Devi, T. Furtenbacher, J. J. Harrison, J. M. Hartmann, A. Jolly, T. J. Johnson, T. Karman, I. Kleiner, A. A. Kyuberis, J. Loos, O. M. Lyulin, S. T. Massie, S. N. Mikhailenko, N. Moazzen-Ahmadi, H. S. P. Müller, O. V. Naumenko, A. V. Nikitin, O. L. Polyansky, M. Rey, M. Rotger, S. W. Sharpe, K. Sung, E. Starikova, S. A. Tashkun, J. V. Auwera, G. Wagner, J. Wilzewski, P. Wcisło, S. Yu, and E. J. Zak, "The HITRAN2016 molecular spectroscopic database," J. Quant. Spectrosc. Ra **203**, 3–69 (2017).